Journal of Nondestructive Evaluation (2025) 44:110
https://doi.org/10.1007/s10921-025-01231-8

Multiscale Characterization of Additive Manufacturing Components with Computed Tomography, 3D X-ray Microscopy, and Deep Learning

Herminso Villarraga-Gómez[1] · Paul Brackman[1] · Amirkoushyar Ziabari[2] · Obaidullah Rahman[2] · Zackary Snow[2] · Ravi Shahani[3] · Katrin Bugelnig[4] · Andriy Andreyev[5] · Yulia Trenikhina[5] · Nathan Johnson[5] · Hrishikesh Bale[5] · Julian Schulz[6] · Edson Costa Santos[6]

Received: 15 May 2025 / Accepted: 29 June 2025

Abstract

Additive manufacturing (AM) facilitates the creation of complex-geometry parts, driving advancements in lightweight aerospace components, high-efficiency engine cooling channels, and customized medical implants. However, ensuring the quality and reliability of AM parts remains challenging due to internal defects, surface irregularities, porosity, and residual trapped powder, which are often inaccessible to traditional inspection methods. Recent developments in X-ray computed tomography (XCT) and 3D X-ray microscopy (XRM), particularly systems equipped with resolution-at-a-distance (RaaD™) capabilities, enable high-resolution, non-destructive evaluation of AM components across multiple scales, from sub-micrometer to macroscopic levels. This paper explores modern XCT and XRM techniques for multiscale characterization of AM parts, focusing on their ability to detect and analyze defects such as porosity, cracks, inclusions, and surface roughness, while offering insights into defect formation mechanisms, material properties, and process-induced variations. The integration of deep learning (DL) frameworks, including Simurgh, DeepRecon, and DeepScout, enhances XCT/XRM workflows by reducing scan times, improving resolution recovery, and enabling accurate defect detection even with limited projection data. These DL-based methods overcome limitations of traditional reconstruction techniques, enabling faster, more reliable characterization of dense materials like Inconel 718 and novel alloys such as AlCe. Applications include process parameter optimization, high-throughput quality control, and multistage AM process evaluation, with DL-enhanced workflows accelerating analysis times from weeks to days. Correlative imaging approaches further validate XCT and XRM data against scanning electron microscopy (SEM) images of physically sectioned samples, confirming the accuracy of DL-based reconstructions and enabling comprehensive defect analysis. While challenges remain in generalizing DL models to diverse materials and imaging conditions, improvements in resolution, noise reduction, and defect detection highlight the transformative potential of these methods. This multiscale and correlative approach enables precise identification and correlation of microstructural features with the overall performance of AM components. By integrating advanced XCT, XRM, and DL techniques, this paper demonstrates a significant leap forward in AM characterization, offering valuable insights into the relationships between processing parameters, microstructure, and part performance, and driving innovations that enhance the quality and reliability of AM products for demanding industrial applications.

Keywords X-ray microscopy · Computed tomography · Non-destructive evaluation · Additive manufacturing · Deep learning

✉ Herminso Villarraga-Gómez
herminso.gomez@zeiss.com

[1] Carl Zeiss Industrial Quality Solutions, LLC, Wixom, MI, USA

[2] Oak Ridge National Laboratory, Oak Ridge, TN, USA

[3] Constellium Technology Center, Voreppe, France

[4] German Aerospace Center DLR, Cologne, Germany

[5] Carl Zeiss X-ray Microscopy, Inc, Dublin, CA, USA

[6] Carl Zeiss Industrielle Messtechnik GmbH, Oberkochen, Germany

Published online: 18 August 2025

1 Introduction

AM has advanced significantly, enabling the production of industrial components with intricate geometries directly from digital design models, eliminating the need for dedicated tooling. This capability holds transformative potential for industries like aerospace and automotive by enabling the creation of highly customized parts tailored to specific applications. However, the presence of internal features within these components poses challenges to traditional quality control methods, as they are often inaccessible to vision-based or tactile inspection techniques. While destructive testing methods can provide measurements of internal characteristics, they often compromise the very features being assessed during the disassembly process.

To address this, X-ray based inspection has emerged as a powerful, non-destructive alternative for examining the internal structures of AM components. This technique can provide critical insights into various aspects of structural integrity, including tolerance limits, residual stresses, dimensional deviations, and internal defects such as cracks or voids that could compromise the performance of AM components and introduce risks of failure. Given that comprehensive literature reviews on the application of X-ray technologies for the inspection of AM parts and processes are readily available in existing literature (e.g., see [1–5]), this section specifically focuses on elucidating the primary conceptual distinctions between XCT and 3D XRM. A preliminary version of this paper was presented in recent conference proceedings [6]. Most industrial XCT systems employ a high-energy X-ray source paired with a flat panel detector to capture projection images of an object as it undergoes rotation on a precision-engineered turntable. This setup is designed to optimize the imaging process by ensuring that high-quality radiographs are obtained from multiple angles. During a complete 360º rotation, or alternatively a 180º rotation combined with the fan or cone angle of the X-ray beam, a series of projection images are acquired. These images are subsequently processed using advanced reconstruction algorithms, such as filtered back-projection or iterative reconstruction techniques, which convert the stack of two-dimensional (2D) radiographic data into a comprehensive three-dimensional (3D) representation of the object. The resulting 3D image is composed of volumetric elements known as voxels, each assigned a specific grey level that corresponds to the density and material composition of the object's internal and external features. This voxel-based representation provides a detailed volumetric map of the object's components, facilitating the identification and analysis of structural characteristics. Advanced image processing techniques further enable the segmentation of specific features within the dataset, while false-color mapping can highlight different materials or density ranges [7]. This enhances both qualitative assessments, such as identifying defects, and quantitative analyses, such as measuring porosity. These capabilities contribute to a deeper understanding of the object's integrity and performance. An illustration of the XCT data process is provided in Fig. 1.

Traditional flat-panel XCT systems primarily rely on basic geometric magnification principles, which are inherently dependent on the sample size as well as the relative distances between the X-ray source, the sample, and the detector. However, this reliance on geometric magnification can impose significant limitations on the size of samples that can be effectively scanned, particularly when analyzing small features within AM components. Micro-geometries

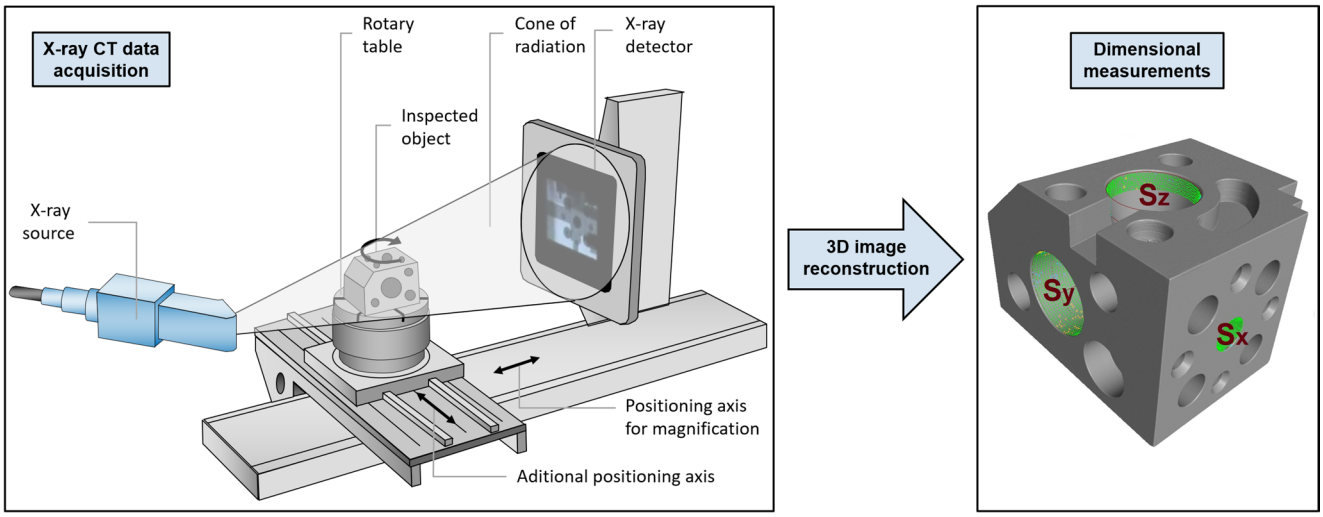

Fig. 1 XCT measurement workflow: A systematic approach outlining the sequential steps involved in capturing radiographic projections for three-dimensional (3D) XCT image reconstruction. After determining the object's surface, a detailed inspection of its geometric dimensions is conducted using a probing and sampling strategy applied to the 3D XCT data. Adapted from [8]

are the most critical, as the most challenging features to analyze are those with dimensions comparable to the voxel size. As the sample size increases, geometric magnification decreases, resulting in a corresponding reduction in image resolution. This limitation poses a significant challenge for researchers and engineers who require high-resolution imaging to accurately assess the integrity and characteristics of complex geometries commonly found in AM parts.

To address these limitations, 3D XRM systems have been developed. These advanced systems integrate both geometric and optical magnification techniques, along with a key feature known as 'resolution-at-a-distance (RaaD)' [9–11]. In the context of XCT, the reduction in geometric magnification when scanning larger samples typically leads to a decline in spatial resolution. However, the incorporation of optical magnification in XRM systems mitigates this issue by maintaining or even enhancing spatial resolution, thereby providing a more detailed view of the sample's internal structures. The integration of RaaD capabilities into the design of XRM systems allows for significant improvements in imaging quality without imposing strict restrictions on the size of the samples being analyzed. This advancement enables researchers to investigate larger components while still capturing fine details, broadening the applicability of XCT across various fields, including materials science and engineering. An illustration of the XRM data acquisition workflow is provided in Fig. 2.

2 Assessing AM Processes Parameters and Quality Using XCT and Deep Learning

The integration of DL techniques into XCT for industrial applications has led to significant advancements in image reconstruction, segmentation, and feature characterization, as highlighted in a recent review [12]. This review outlines key challenges in XCT inspections, such as time constraints and image artifacts, and emphasizes the need for greater automation in data processing. It identifies well-developed machine learning and DL methods in segmentation and feature extraction, while calling for future research to focus on techniques that enhance raw measurement data and reduce the reliance on labelled datasets. Additionally, it advocates for incorporating uncertainty quantification and explainable artificial intelligence to improve the robustness and adoption of these technologies in non-destructive testing and metrology.

A common challenge in applying DL techniques to XCT is the lack of pre-existing training data. Many DL methods required models to be pre-trained on labeled datasets, but the complexity and diversity of XCT data make training a generalized model difficult. A more effective approach is to train the model directly on the specific XCT data that the user is trying to reconstruct. This approach offers the significant advantage of enabling model training to improve scan quality using automatically captured reference scans, thereby removing the need for human-annotated data in

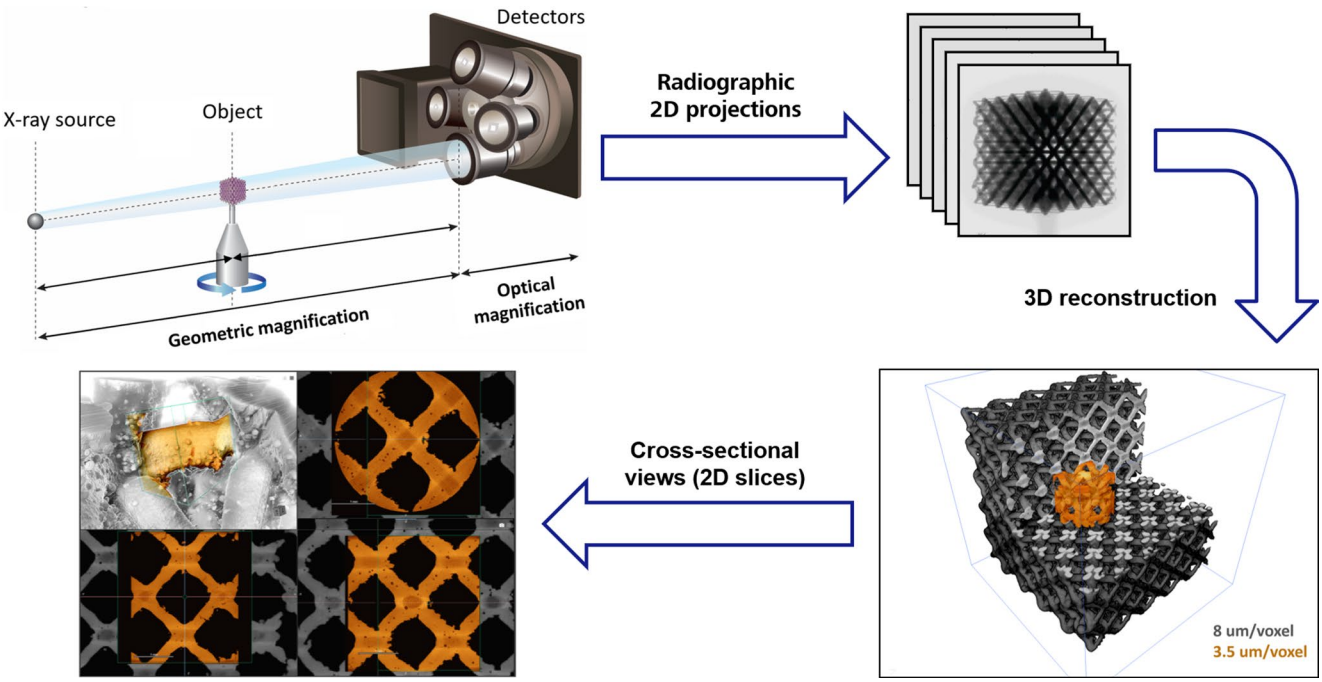

Fig. 2 XRM measurement workflow: Integration of geometric and optical magnification to enhance the spatial resolution capabilities of 3D XCT image reconstruction. The bottom row displays combined data for reconstructing an AM lattice from two distinct scans: a full field-of-view scan at 8 µm per voxel and an interior tomography scan obtained at 3.5 µm per voxel

applying DL for anomaly detection in XCT. Additionally, it can drastically reduce scanning time—by minimizing the required number of projections and exposure duration—while simultaneously enhancing the quality of XCT reconstructions.

One notable implementation of this strategy is Simurgh, a DL-based XCT reconstruction framework designed to overcome the limitations of traditional analytical and iterative methods [13–15]. Simurgh employs a combination of real XCT scans and physics-informed synthesis for training [14, 16]. In the case of real scans, dense XCT scans of actual components are used, incorporating physics-based beam hardening corrections and model-based iterative reconstruction (MBIR) techniques [13, 17] to generate high-quality training datasets. These dense datasets are then subsampled to create low-quality input data, forming low-high quality pairs. By augmenting these pairs, Simurgh trains a robust supervised 2.5D convolutional neural network (CNN) capable of producing high-quality reconstructions during inference, even for scans performed at significantly reduced durations.

Alternatively, Simurgh leverages synthetic data by combining defect libraries from previous XCT scans, CAD models of parts, and physics-informed simulators (e.g. the ASTRA toolbox [18]) with generative adversarial networks (GANs) [14, 19]. This approach generates realistic training data pairs to train the 2.5D CNN for high-resolution 3D reconstructions from sparse or short-duration scans. Additionally, the combination of real and synthetic data has been used in prior studies [16] to address challenges such as scattering artifacts. The result is a substantial reduction in scanning time, cost, and labor, while improving defect detectability and maintaining high image quality.

Simurgh exemplifies the potential for future research to address key gaps identified in the literature, particularly in enhancing raw measurement data and automating the inspection process. This framework demonstrates how DL can significantly enhance XCT workflows, making them faster, more efficient, and more accessible for industrial applications. Simurgh has been applied across a range of materials for high-throughput inspection and characterization of dense AM metal parts, facilitating process parameter optimization for challenging materials such as AlCe, 316 L/H, and Inconel 718 [13, 14, 20–22]. While its primary focus has been on accelerating scan times for dense metallic parts and reducing artifacts such as noise, beam hardening, streaks, and scattering, the method is sufficiently adaptable to be extended to other material classes, such as polymers, provided it is trained on appropriate materials and scans.

Example results for AlCe and Inconel 718 alloys are presented in Fig. 3(a) and Fig. 3(b), respectively. In Fig. 3(a), an AlCe alloy sample was scanned using a ZEISS Metrotom 800 system. A typical scan duration of 39 min was reduced to 13 min using Simurgh, representing a 3x speed improvement [13, 14]. A representative reconstruction slice is shown alongside high-resolution microscopy, which

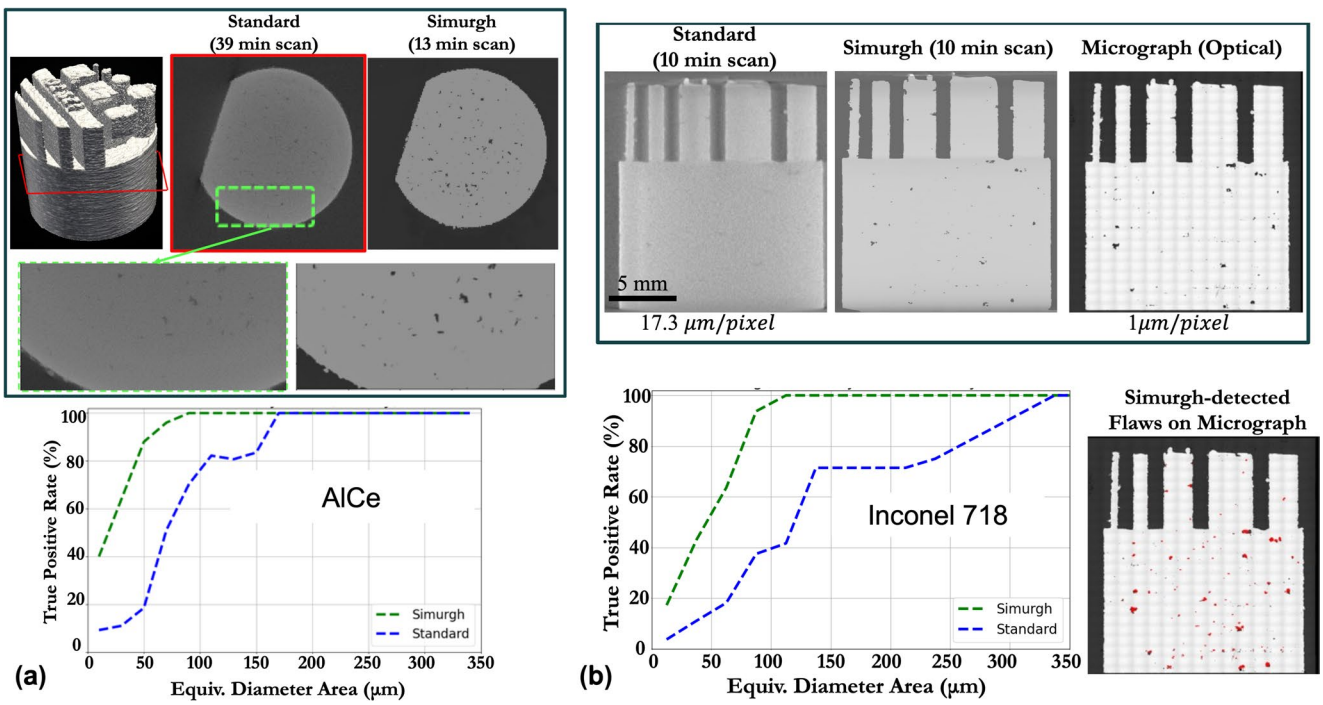

Fig. 3 An example of Simurgh's performance on in-distribution data (test data from materials and scans similar to those used during training). Comparison with high-resolution optical microscopy was employed to calculate the true positive rate (flaw detection probability) [13]. (**a**) For Aluminum Cerium (AlCe) alloy (density ~3.4 g/cm³); (**b**) For the very dense Inconel 718 alloy (density ~8.5 g/cm³)

verifies that Simurgh achieves a true positive rate exceeding 90% for detecting flaws larger than 50 µm. Scanning Inconel alloys poses an even greater challenge due to their high density. Conventional methods often require over two hours to scan a 15 mm sample, but Simurgh enabled high-quality reconstruction from a 10-minute scan (Fig. 3(b)), achieving comparable detection accuracy [21, 22]. This is particularly significant for dense materials, where scattered radiation typically reduces contrast and limits the identification of small defects. Scattering artifacts distort local gray values, making reliable identification of small defects more difficult. Simurgh effectively addresses these challenges, enabling faster and more accurate defect detection in dense materials.

The effectiveness of the Simurgh framework is demonstrated through a comparison of defects identified in its reconstructions with those observed in optical micrographs, which serve as the ground truth. A strong overlap between pores visible in the XCT data and the micrographs confirms Simurgh's ability to produce high-quality representations. In the examples shown in Fig. 3, samples were sectioned, and optical microscopy was performed at a resolution of 1 µm. Flaws such as pores and cracks were segmented in both the XCT and microscopy datasets, which were registered using the procedure outlined in Ref [13]. The True Positive Rate (TPR)—the ratio of flaws detected in both XCT and optical microscopy—was calculated using the registered datasets. Results show that Simurgh significantly improves flaw detection, even for scans performed at much faster rates than conventional methods.

For instance, scanning a 15 mm AlCe sample typically takes 40 min to 1 h, while dense materials like Inconel 718 require over 2 h to achieve high-quality scans capable of detecting small flaws. These extended durations are primarily attributed to the material's density and the need to meet the Nyquist criterion, which often demands nearly the same number of projection views during a scan as the number of detector columns to ensure high-quality reconstruction when employing the standard analytical Feldkamp-Davis-Kress (FDK) algorithm [23]. For instance, approximately 2000 projection views are required for standard reconstructions involving around 2000 detector columns [24, 25]. Simurgh overcomes these limitations, enabling faster scans without compromising detection accuracy. Additionally, Simurgh's high-quality reconstructions simplify post-processing, significantly reducing the total inspection effort. This capability supports the use of XCT as a tool for process parameter optimization, where hundreds of samples—each printed with different parameters—can be scanned rapidly and analyzed for flaw density and geometric accuracy [14, 20–22, 26].

Supervised deep learning models, such as Simurgh, typically require the test data to closely match the training data in terms of material properties, scanner type, resolution, and scan settings. This study evaluates Simurgh's ability to generalize beyond its original training data distribution. To test this, a new Simurgh model was trained using data from four materials —AFA, 718, Ti64, and AlSiMg—scanned on the ZEISS Metrotom 800 at a voxel resolution of 17.3 µm. High-fidelity scans reconstructed using the BHCN-MBIR method [17] were used as ground truth data. Corresponding sparse-view reconstructions, generated using the FDK algorithm with 145–250 projection views, were created to train the model on low-to-high quality volume pairs. This training approach enabled the model to enhance sparse-view reconstructions, producing high-quality results even with limited projection data.

The trained Simurgh model was then applied to samples made of Aheadd CP1 (AA8A61.50), a novel aluminum alloy developed by Constellium for the high solidification rates of laser powder bed fusion AM [27]. These samples were scanned using the ZEISS Metrotom 1500 system under the following conditions: 800 projection views, 1-second integration time, 2x binning, no image averaging, and a voxel size of 16.1 µm. The Metrotom 1500, equipped with a larger detector (139×139 µm² pixels), was operated at different voltages and currents, resulting in varying spot sizes and signal characteristics. To evaluate Simurgh's performance on this out-of-distribution (OOD) dataset, the reconstructions were compared against synchrotron XCT data acquired at a 5 µm resolution. Although the synchrotron reconstructions presented their own challenges, such as paste residue artifacts, they provided high contrast around pores, making them suitable ground truth references. For additional comparison, industry-standard FDK reconstructions were also included as a baseline for comparison. All datasets—FDK, Simurgh, and synchrotron—were segmented using a deep learning-based flaw segmentation model. Segmentations were registered to the synchrotron data using fiducial landmarks and iterative closest point (ICP) alignment [29]. Despite registration challenges due to paste artifacts, the alignment was sufficient to evaluate segmentation accuracy. Defect detection performance was quantified using precision, recall, and F1-score metrics. The F1-score, defined as $F1 = \frac{2TP}{2TP+FP+FN}$, balances the trade-off between true positives (TP), false positives (FP), and false negatives (FN). Figure 4 highlights Simurgh's superior reconstruction quality (Fig. 4(b)) compared to synchrotron data (Fig. 4(a)), with F1-scores plotted against flaw diameter (Fig. 4(c)) showing that Simurgh significantly outperforms the standard FDK, even on OOD data.

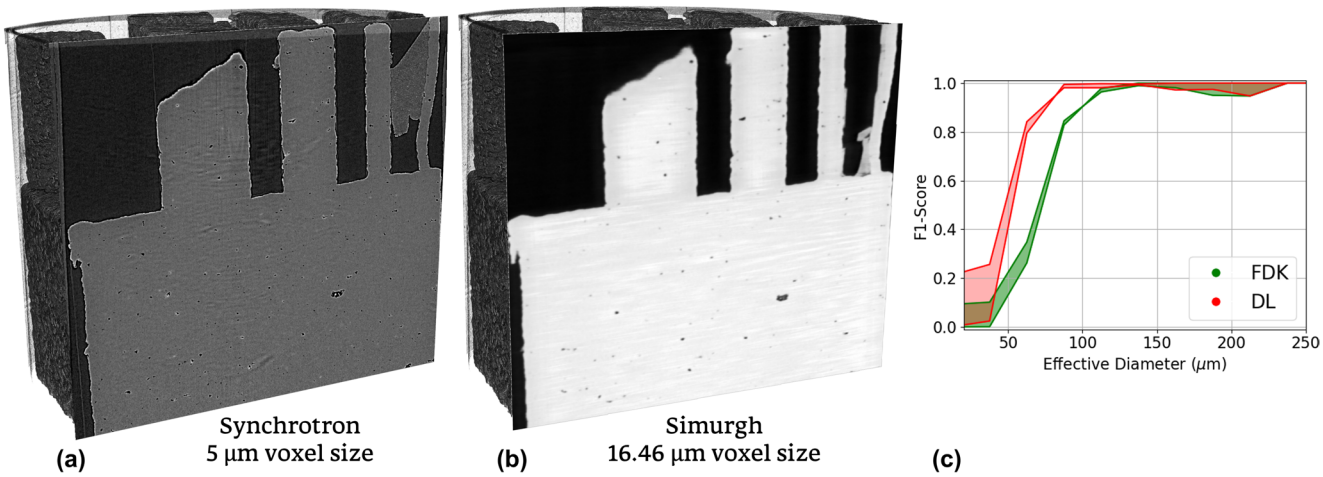

Fig. 4 Performance of the Simurgh Model on OOD data, compared with synchrotron data. (**a**) Slice through the 3D synchrotron volume; (**b**) Simurgh deep learning (DL) reconstruction of the volume; (**c**) F1-score comparison between Simurgh results and standard reconstruction for a fast sparse scan

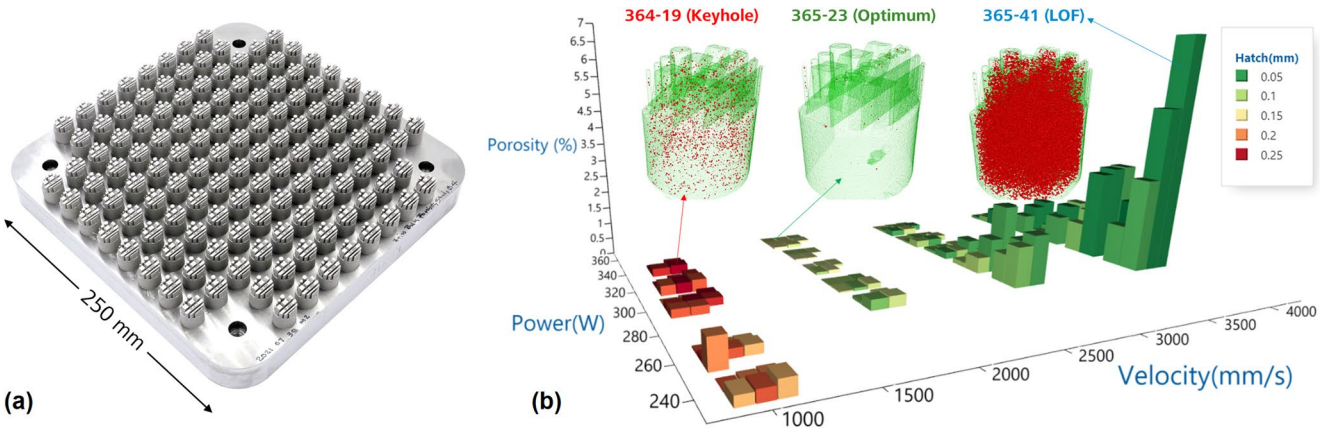

Fig. 5 (**a**) AlCe AM build plate filled with testing coupons; (**b**) process parameter mapping based on XCT data for developing a new AlCe AM alloy (Adapted from Ref. [13]). Deep learning (DL)-based algorithms enabled sparse XCT scanning and facilitated automated reconstruction and segmentation of porosity flaws.

Simurgh's ability to produce high-quality reconstructions from accelerated scans, facilitates process parameter optimization for novel metal AM materials. For example, it was used to identify optimal AM process parameter for CP1 using 90 µm layers on a 700 W SLM280 printer [30]. Additionally, a high-throughput AM print quality assessment system based on C-scan ultrasonics has shown promising results on CP1, complementing Simurgh XCT's capabilities [31, 32]. Simurgh's strong performance on OOD datasets is attributed to its training on diverse materials, varied scan settings, and extensive data augmentation. However, as a supervised learning framework, its performance is inherently limited by its training domain. Significant deviations, such as more complex or denser geometries, different scan parameters (e.g., integration time or number of projection views), or the presence of anomalous inclusions and secondary materials, may degrade reconstruction quality and require retraining. Similarly, while the model performs well on resolutions near its training voxel size, substantial deviations may necessitate new models optimized for different resolution domains. Addressing these challenges to enhance Simurgh's generalizability and robustness beyond its current operating envelope remains a focus of ongoing and future research [16, 33, 34].

XCT can be effectively used to rapidly evaluate the outcomes of hundreds of AM print parameters, such as laser power, velocity, hatch spacing, and gas flowrate, to optimize settings for specific material and machine combination (e.g., see Fig. 5). The workflow for analyzing printing parameters begins with the fabrication of test coupons, as shown in Fig. 5(a). These cupons can either be built using uniform parameters or designed with a parameter grid. Once the coupons are removed from the build plate, XCT scanning is performed automatically, followed by the subsequent

analysis. By leveraging DL-based methods [13], this process has been accelerated dramatically, reducing the evaluation time for a metal AM test plate from up to six weeks (using 2D light microscopy) to just one or two days.

DL-based methods achieve this acceleration by enabling shorter XCT scan times and requiring significantly fewer projections—down to as low as 1/10th of the total projections typically needed in traditional methods, which often require over a thousand projections per scan. These methods also reduce image noise and XCT artifacts, enhancing the accuracy of defect alignment and segmentation in subsequent analysis steps. This efficiency is critical, as large sample volumes must be scanned to derive meaningful insights into AM processes. Reducing the number of projections for XCT data reconstruction directly decreases measurement acquisition times and, consequently, the cost of the measuring process [24]. For dense materials like Inconel, scans that traditionally required 1800–2000 projection views can now be performed with only 145–200 projection views, thanks to DL-enhanced reconstruction techniques.

Theoretical limits on the minimum number of projection views for accurate CT reconstruction are derived from the Nyquist-Shannon sampling theorem [25]. By pushing these limits, DL-based methods enable faster scans without compromising reconstruction quality. The speeds achieved in this workflow suggest that replacing samples during a series of XCT scans could become the bottleneck in the process. This limitation can be addressed by integrating an autoloader or automated sample changer, ensuring seamless workflow continuity.

Beyond scan times, the consistency of DL-based reconstructions significantly reduces post-processing efforts. Traditional FDK-based reconstructions often suffer from inconsistencies and artifacts, requiring manual tuning of segmentation parameters for each sample. This manual effort wastes time and labor. In contrast, Simurgh's high-quality and consistent reconstructions allow the use of a single segmentation model with fixed parameters across all samples. This consistency enables fully automated post-processing and analysis, saving substantial time and facilitating high-throughput process parameter optimization.

From a computational perspective, the use of graphics processing units (GPUs) ensures rapid inference times, typically ranging from 1 to 10 min depending on sample size and GPU availability. Even for longer Simurgh's inference times, the workflow remains efficient by running reconstructions concurrently with the scanning of the next batch of samples. This parallelized approach ensures uninterrupted high-throughput parameter optimization.

In summary, the combination of reduced scan times, automated workflows, consistent reconstructions, and optimized computational processes provides a scalable and efficient methodology for AM parameter optimization. This approach accelerates evaluation, reduces labor and operational costs, and serves as a valuable tool for advancing AM technologies.

The Design-of-Experiment (DOE) analysis for an AlCe alloy, shown in Fig. 5(b), illustrates how the porosity levels vary with changes in energy density during processing. This enables the experiment designers to identify optimal processing conditions for new alloys. Beyond determining AM process parameters, the workflow described in Ref [13] can also assess the repeatability of an AM process by analyzing coupons produced across different builds or machines. Individual test coupons (small stubs visible in Fig. 5(a)) can be further inspected to verify scan quality and analyzethe types of porosity formed during manufacturing.

Figure 6(a) presents a 2D slice from the 3D volume dataet of a test coupon scanned in the fast parameter analysis workflow. This workflow effectively detects layer defects, lack of fusion, keyhole pores, cracks, and surface characteristics. After confirming the scan and segmentation quality, test parts were produced using the optimized parameters identified in the workflow. Figure 6(b) shows a transverse slice of a printed part containing a layer defect formed during processing. Such defects render the part unsuitable for further testing and development.

Layer defects typically arise when the powder spreading step encounters a raised region, leading to sparse powder distribution in specific areas of the part. Although these defects are not visible on the surface, they significantly compromise the part's performance. Layer defects may occur in isolated locations or intermittently throughout the built, as shown in Fig. 6(c-d), with each defect acting as a potential failure initiation site. When defects appear at regular intervals, this could indicate a powder shortage from the spreader, warranting an investigation into the 3D printers recoating mechanism.

The DOE workflow not only aids in optimizing AM process parameters but also provides critical insights into defect formation and process repeatability. By identifying and addressing issues such as layer defects, the workflow ensures higher part quality and performance, making it an invaluable tool for advancing AM technologies.

3 Characterization of AM Components with XCT and 3D XRM

3D XRM is instrumental in analyzing AM powders, enabling detailed characterization of particle size, shape, and inclusions. High-resolution scans are especially crucial for fine powders used in processes such as Powder Bed Fusion (PBF) and Binder Jetting, as these powders are prone to

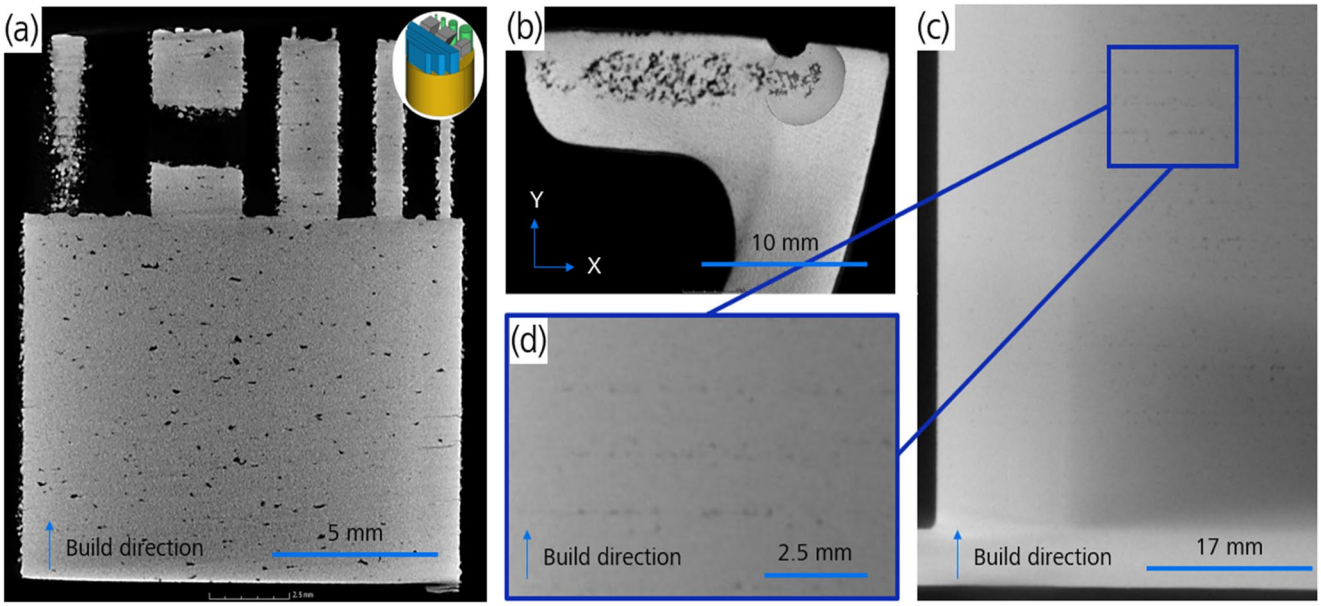

Fig. 6 (**a**) XCT slice of an AlCe AM test coupon revealing large pores ready for segmentation and comparison with other parts in the build. (**b**) XY slice of a part showing a large layer defect from a top-down view found during part inspection. (**c**) Layer defects viewed from a slice transverse to the build direction with (**d**) an inset box showing a higher magnification of the region of interest

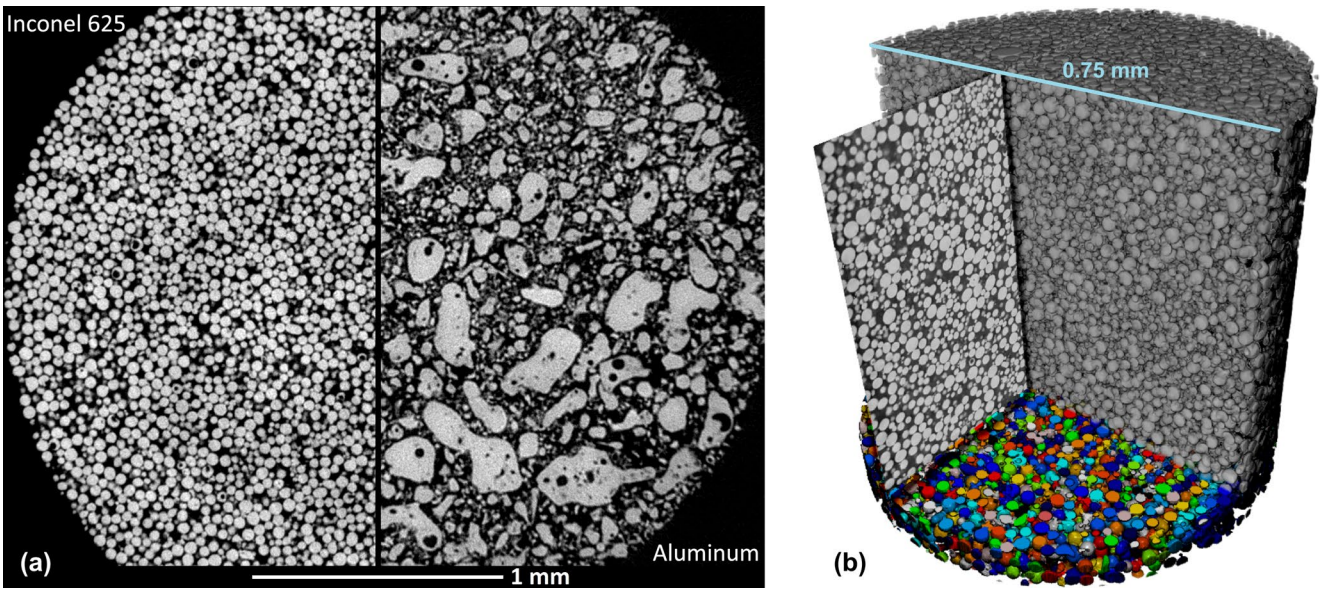

Fig. 7 (**a**) A composite XCT image of two distinct raw AM powders (adapted from [40]), illustrating the size and shape distribution of powder grains, the presence of satellite particles, and internal porosity within individual grains. (**b**) Volumetric reconstruction of Ti6Al4V AM feedstock powder scanned with a 3D XRM (ZEISS Xradia 620 Versa), highlighting the size and shape distribution of the powder grains

internal voids and inclusions that can compromise the quality and mechanical properties of the final parts.

For example, Fig. 7 illustrates that most aluminum powder grains are non-spherical, vary in size, and exhibit irregular morphologies. These characteristics negatively affect the powder's spreadability and flowability, which, in turn, can compromise print quality. Characterizing the sphericity and size of powder grains, as well as understanding the relationship to functional printing conditions, is critical for determining the limits of powder recycling and ensuring optimal performance.

In contrast, Inconel powders appear as consistently spherical grains that are nearly identical in size, and relatively small compared to aluminum grains. However, some Inconel grains still exhibit micro-porosity structures. The presence of these channels or microstructures in the powder

material could influence the porosity percentage of a finished AM part made from such material or induce fractures and cracks due to the lack of fusion voids, as illustrated in Fig. 8. Such defects can significantly compromise the structural integrity and reliability of the printed components.

Beyond porosity, other critical attributes of AM powders require thorough evaluation to ensure process reliability and part quality. These include particle size distribution, morphology, heterogeneity, geometry, and grain microstructure [35–39]. Metal AM powders generally range in size from 15 μm to 150 μm [35]. Certain anomalies within the powder can induce defects in the final AM parts. For instance, powders with a uniform size distribution promote homogeneous melting and facilitate strong interlayer bonding [37]. Conversely, irregularly shaped particles or grain agglomerates can lead to porosity in the final component, particularly in laser or electron beam melting processes. These anomalies also affect flowability and packing density, negatively impacting print quality. High-resolution 3D XRM scans can identify these anomalies, enabling powder optimization before the AM process begins. This ensures that the powders used are of the highest quality, minimizing the risk of defects and enhancing the overall reliability and performance of AM components.

As mentioned in Sect. 1, traditional XCT systems using simple geometric magnification have limited spatial resolution for visualizing small features within AM parts, and resolution deteriorates as sample size increases. This limitation can be overcome with 3D XRMs using geometric and optical magnification with RaaD. For example, Fig. 9 demonstrates how RaaD enables multiscale characterization of an AM steel lattice sample. Smaller features, such as trapped powder particles, are clearly visualized with high-resolution XRM scans. An overview tomography scan was first collected using a 0.4X magnification objective (nominal voxel size: 10 μm), followed by a higher-resolution scan with a 4X magnifying objective (nominal voxel size: 4.5 μm). While the powder was visible in the low-resolution scan, segmentation was only possible in the higher-resolution scan, which used a straightforward intensity thresholding method. Unlike traditional inspection methods requiring physical sectioning, 3D XRM provides a non-destructive, comprehensive view of both external and internal geometries, enhancing defect detection and analysis.

By performing scans at different resolutions, researchers and engineers can reconstruct a detailed multiscale image reconstruction of a part, capturing both macro-structures and micro-defects. High-resolution scans reveal small-scale defects, while lower-resolution scans capture the overall geometry. The resulting 3D model enables defect identification without physical sectioning, providing a more efficient and complete evaluation of AM components.

Understanding the relationship between defects, material properties, and input process parameters is critical for determining whether an AM component should pass or fail quality assessments. Defects such as porosity, inclusions, trapped powder, and surface irregularities can significantly degrade mechanical performance, particularly

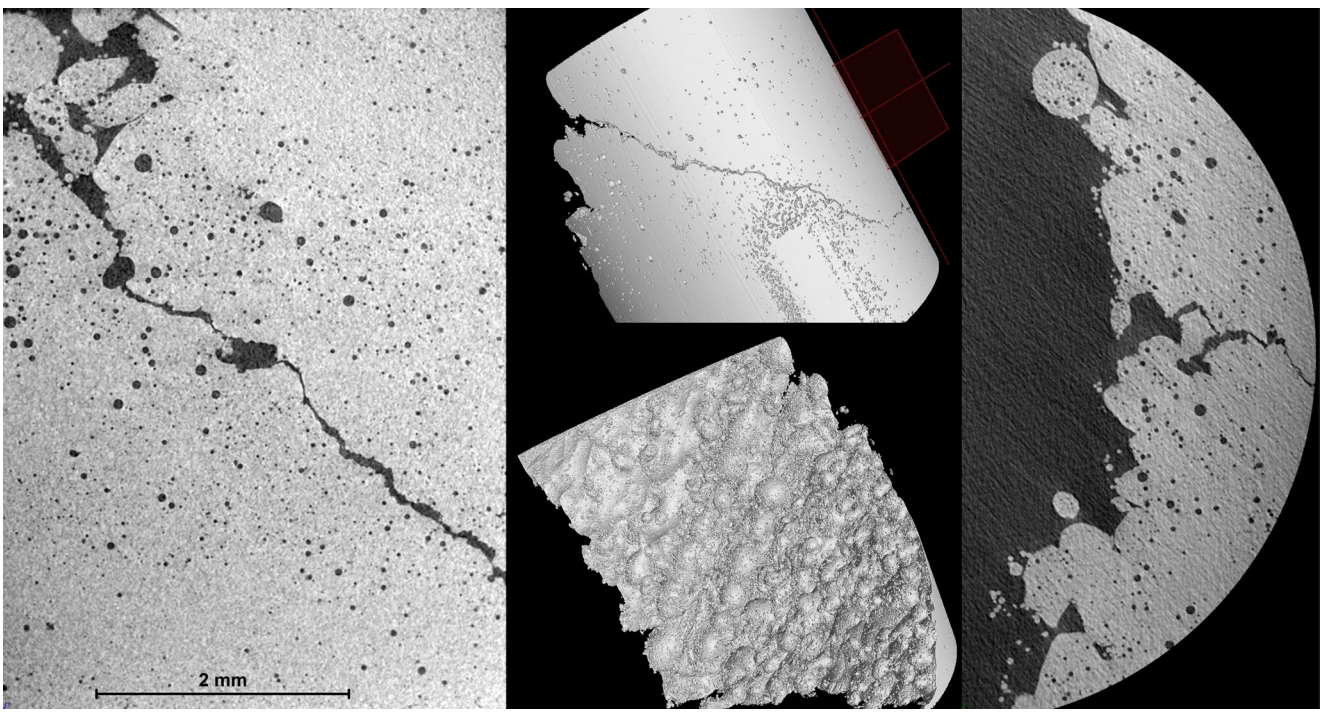

Fig. 8 Crack formation due to interconnected porosity within an AM aluminum part, scanned with a 3D XRM (ZEISS Xradia 620 Versa)

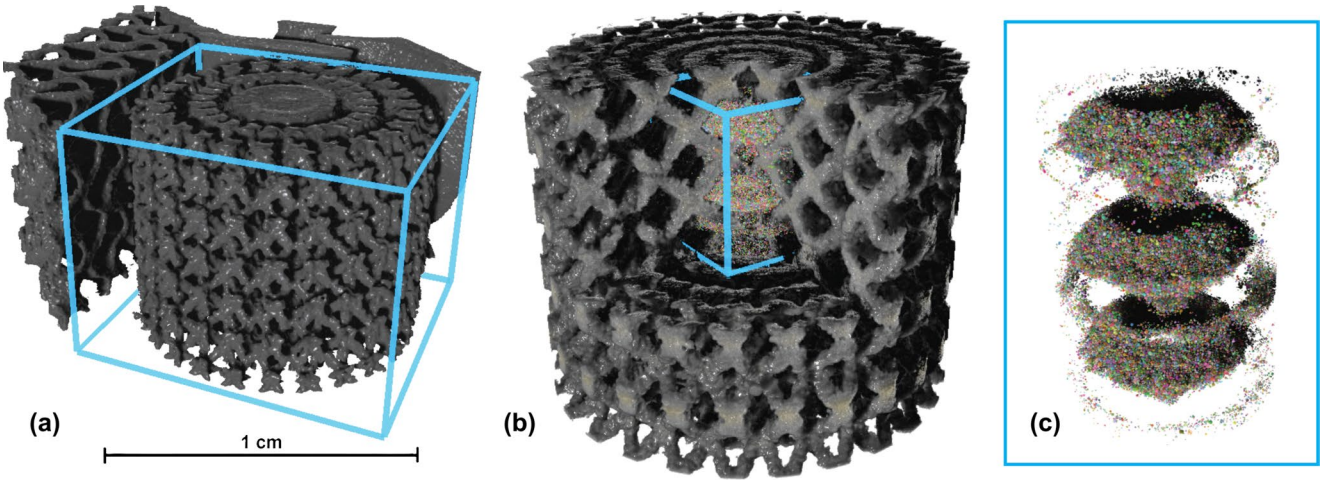

Fig. 9 Multiscale characterization of an AM steel lattice featuring agglomerated powder (unmelted particles) trapped within. Regions of interest in the lattice were scanned using various zoom lenses with a 3D XRM equipped with RaaD capabilities (ZEISS VersaXRM 730). (**a**) Overview tomography of the lattice obtained with a 0.4X zoom lens. (**b**) Interior tomography of the lattice captured with a 4X zoom lens, revealing trapped powder within the lattice interior. (**c**) Segmentation and isolation of the trapped powder. Coloration of the powder particles is for illustrative purposes only

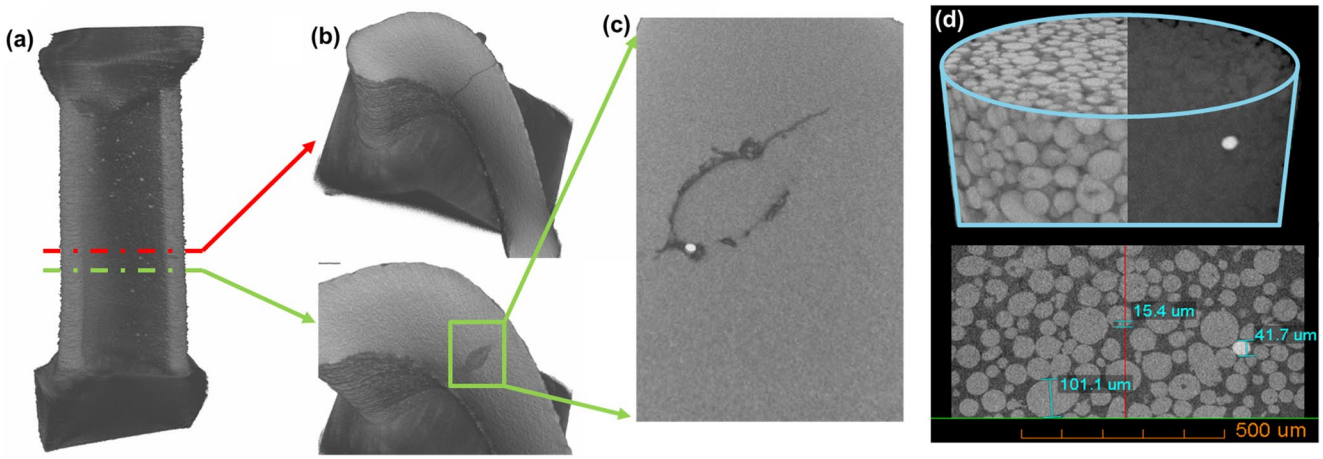

Fig. 10 (**a**) 3D rendering of XCT reconstruction of an Inconel-738 AM turbine blade. (**b**) Detailed views showing cracks (top) and lack-of-fusion defects (bottom). (**c**) Zoomed-in XRM data highlighting a high-density unfused powder particle. (**d**) XRM scan revealing high-density particle contamination in the AM powder

under cyclic loading conditions where fatigue properties are critical. A thorough analysis of these defects and their influence on material behavior is imperative. Establishing a robust baseline for determining acceptable defect thresholds may require additional testing and advanced analytical techniques, such as high-resolution 3D XRM imaging to detect and quantify defects, followed by mechanical testing to assess their impact on performance. Computational modeling and advanced statistical methods can further aid in predicting the effects of defects on the structural integrity of AM components.

Foreign materials in printed components can act as crack initiation sites or exacerbate internal defects. For example, Fig. 10(a-c) show cracks and non-fusion defects surrounding an internal contaminant in an Inconel-738 turbine blade. High-density contaminants often result from improper powder handling, inadequate machine cleaning between build cycles, or substandard raw materials. Such contamination can be identified by inspecting incoming AM powder at various stages of the build process, as illustrated in Fig. 10(d). Defects like inclusions and porosity can reduce mechanical properties, particularly fatigue resistance in turbine blades. Additionally, understanding powder microstructure—such as grain size and shape —is crucial for predicting and controlling the mechanical properties of the final product. High-resolution 3D XRM offers a non-destructive method to analyze these features, providing valuable insights for

optimizing powder selection and processing of specific AM applications.

More broadly, testing and qualifying AM processes is fundamental for understanding how defects affect structural performance and the quality of both raw materials and finished products [41–44]. For instance, XCT data has proven effective in studying the transfer of properties and characteristics from a "witness coupon" to a component. A turbine blade and an AM cylindrical rod, acting as a witness coupon, are often manufactured simultaneously from the same material to enable direct property comparisons. Initial studies [5, 44] suggest that non-fracture-critical properties are less sensitive to defect distribution than fatigue properties, underscoring the importance of defect characterization in fatigue-critical applications.

XCT has proven effective in detecting defective blades, enabling the successful production of crack-free Inconel-738 turbine blades via PBF. These blades were machined to tolerance and hot-fired during an engine performance validation trial [45]. This study involved scanning and inspecting over 100 test turbine blades for cracks. By combining high-resolution XCT imaging of raw feedstock with high-throughput XCT imaging of finished components, a comprehensive characterization strategy for detecting cracks and inclusions was established. This extensive dataset, comprising both defective and non-defective samples, proved valuable for training DL models and validating artifact and noise reduction techniques. Such approaches enable faster scanning times while improving defect detection confidence, paving the way for more efficient and reliable AM workflows.

4 Evaluation of Internal Surface Quality in AM Parts

PBF has proven effective in producing near-net-shape parts, consolidating multiple traditionally joined components into a single AM part. This consolidation simplifies assembly, enhances design flexibility, and minimizes overall material waste. However, variations in surface quality across different AM processes may require surface finish modifications to meet performance requirements. Surface improvements can be achieved through optimized contour parameters during printing or post-processing techniques, which enhance both mechanical properties and aesthetic quality to meet application-specific standards.

The layer-based nature of AM introduces surface roughness, which has been studied using traditional XCT, particularly for large-scale polymer parts [46]. Factors such as inclination angles and layer thickness were varied to produce ramps with different theoretical average roughness (Ra) values. The study revealed that post-processing significantly influences roughness measurements, with distinct effects observed for Polyjet and selective laser sintering (SLS) technologies. Linear roughness parameters were deemed appropriate for fused deposition modeling (FDM) and Polyjet surfaces, while SLS surfaces require areal characterization for accurate assessment. Additionally, XCT-based surface roughness measurements are sensitive to surrounding material thickness [47], as identical surfaces yield varying roughness parameters under different conditions. This highlights the importance of considering material density and artifacts during measurement.

Advanced methodologies integrating XCT with 3D roughness characterization of metal AM channel surfaces have enabled non-destructive analysis of internal AM surfaces [48], facilitating detailed roughness distribution studies. For instance, XCT was employed to compare conventional heating coils with AM counterparts, revealing that brazed defects common in traditional coils are mitigated through AM. Figure 11 illustrates a 2D slice of the XZ-plane, showing a cross-section of the coil and one of the pipes, enabling a direct comparison of the internal structures and defects. Conventional coils exhibit cracks and pores in brazed regions, leading to inconsistent lifecycles, while AM coils produced via laser PBF show improved structural integrity. However, laser PBF surface roughness is influenced by factors such as thermal transfer, particle adhesion, spatter, and layer thickness. Notably, AM parts may exhibit design-related limitations, such as step changes in wall thickness or wavy surfaces from support structures, which require further optimization.

Build orientation in PBF significantly impacts surface quality. Down-facing surfaces often require support structures and post-processing, but internal down-facing surfaces, such as those inside tubes, cannot be mechanically cleaned or visually inspected. To address this, the RaaD capabilities of a 3D XRM (ZEISS Xradia 620 Versa X-ray microscope) were used to "zoom in" on the internal regions of interest and enable high-resolution scans of internal surfaces without sample preparation. Figure 12(a) shows a heating coil in the microscope, where an overview scan is first performed using a 0.4X objective. The overview identifies the transition between upskin and downskin (overhanging surface), and the region of interest is selected (green circle in Fig. 12(b)). The coordinates are then transferred to the 3D microscope for a RaaD scan, which is overlaid on the overview scan in Fig. 12(b) and displayed in 3D in Fig. 12(c). RaaD offers the unique advantage of performing high-resolution scans on intact samples without requiring sample preparation or size reduction, unlike conventional geometric magnification-based XCT scanning approaches. The conventional heat coil pipe was scanned similarly, and its 3D volume is shown in Fig. 12(d). Testing surface

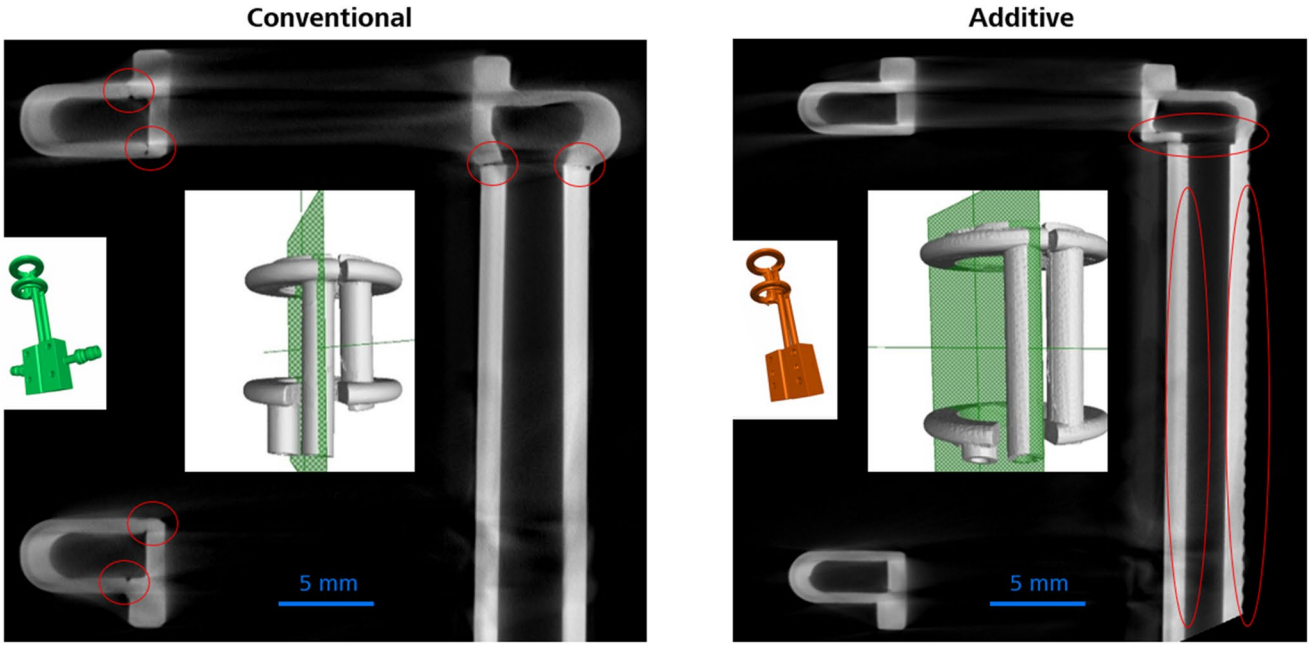

Fig. 11 XCT inspection of induction hardening coils: (left) conventionally produced and (right) additively manufactured

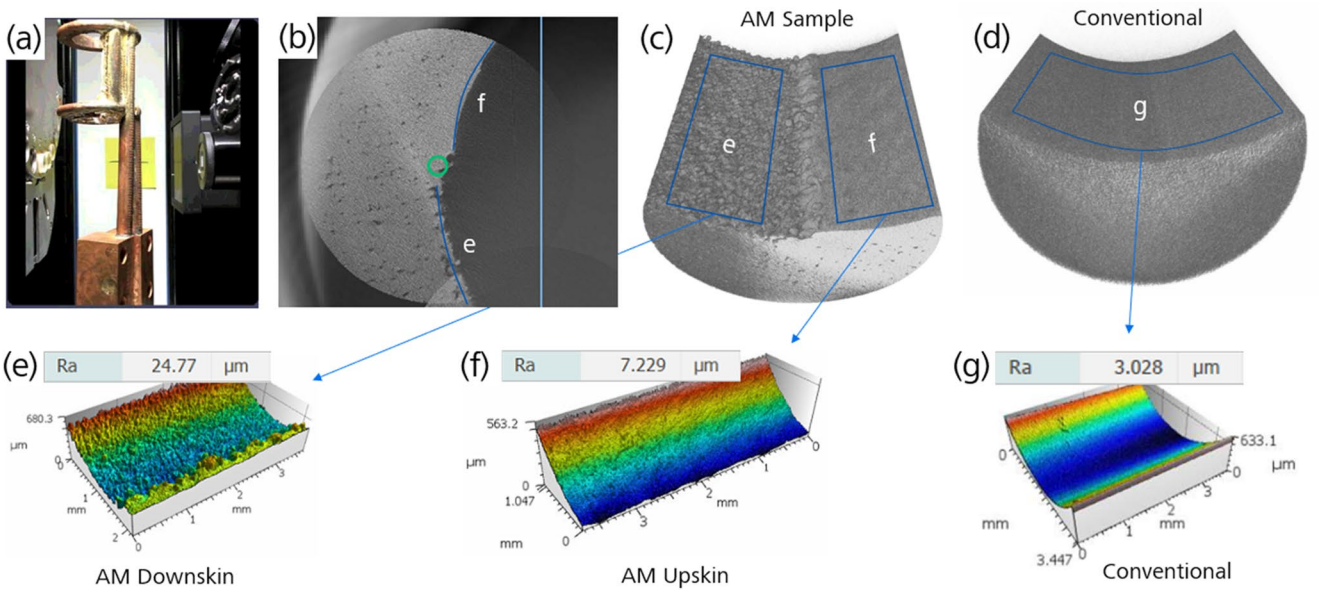

Fig. 12 Workflow for inspecting internal surfaces using 3D X-ray microscopy: (**a**) Part placement, (**b**) View perpendicular to the longitudinal axis, (**c**) AM 3D surface, (**d**) Conventional 3D surface, (**e**) AM downskin, (**f**) AM upskin, and (**g**) Conventional pipe surface

locations were generated from voxel datasets (gray scales or absorption intensities) obtained through XRM scanning, using local adaptive or dynamic gradient threshold methods [49, 50].

From the contrast in 3D volumes, the surface was polygonized with sub-pixel resolution, or sub-voxel interpolation. This involved identifying lines (surfaces in 3D) along the highest brightness gradient in the voxel data, distinguishing the edges between the component's material and the background or surrounding air. A suitable surface path from the region of interest was selected, and the geometry-related curvature was removed by fitting and subtracting a polynomial of appropriate order. A 1D line profile was then extracted to calculate the Ra values, as shown in Fig. 12(e-g). A decreasing trend in roughness was observed, moving from overhanging surfaces to upskin and finally to the conventional copper pipe. Beyond Ra, other surface features, such as reentrant features are critical for classifying internal

surfaces. As complete surface analysis is possible using the XRM data, as shown in Table 1. For instance, consider Rz, which assesses extreme surface height variations, while Rmax is important for applications where the highest peak or deepest valley could affect wear resistance or fatigue life.

Comparative analysis reveals higher surface variation in 3D-printed parts compared to conventional ones. Whether this variation is acceptable depends on the part's application. Internal surfaces can potentially be improved through abrasive etching processes, making non-destructive characterization methods like XCT essential for evaluating etching effectiveness.

5 Multiscale Porosity Analysis Using Deep Learning and Other Tools

As demonstrated through several examples throughout this paper, porosity is a challenging aspect of additive manufacturing that significantly influences the mechanical and thermal performance of an AM part. Achieving tight control over the porosity demands a comprehensive understanding of its distribution, morphology, and sources of origin, which often span multiple length scales, i.e., nm to mm. Detecting porosity across a broad size range in a large representative sample volume is difficult due to the resolution vs. field-of-view (FOV) trade-off. Large FOVs typically reduce imaging resolution, while higher resolution limits the sample volume that can be scanned. In XCT, this challenge is further compounded by X-ray penetration depth limitations in larger samples, which affects the resolution, signal-to-noise, and image quality.

Recent advances in X-ray imaging hardware and DL-based reconstruction methods, such as ZEISS Advanced Reconstruction Toolbox 4.0, offer innovative solutions to these challenges. Improvements in X-ray scintillator technology now enable imaging of denser materials at higher resolutions and X-ray energies. For instance, earlier scintillator-based objectives were limited to 100 kV and 0.7 µm/voxel resolution, restricting high-resolution imaging to small sample sizes (e.g., 1–2 mm of steel). The latest scintillators, coupled with high-magnification objectives (such as the 40X-Prime objective for ZEISS XRMs), enable the extension of the X-ray tube's voltage range up to 160 kV, achieving resolutions as fine as 0.4 µm/voxel. This improvement is attributed to reduced point spread and enhanced sensitivity at higher voltage levels.

Table 1 Characterization of XCT full-profile parameters for internal surfaces derived from the XRM data presented in Fig. 12, in accordance with the ASME B46.1 standard. Roughness parameters (S-L): F: none, S-filter (λs): gaussian, 2.500 µm (1 cut-off), and L-filter (λc): gaussian, 8.000 µm (1 cut-off).

Profile parameters	AM dowskin	AM upskin	Conventional
Ra (µm)	24.77	7.229	3.028
Rz (µm)	252.3	66.24	29.79
Rmax (µm)	284.7	70.58	34.78
Rq (µm)	34.46	9.232	3.838
Rsk	0.3306	0.03025	0.4531
Rku	5.618	3.394	3.946

Despite these hardware developments, mapping submicron voids in larger samples remains challenging due to relatively low signal-to-noise ratios. This study demonstrates a multiscale 3D imaging approach on a 3D-printed Inconel 718 alloy lattice (Fig. 13). The method combines low-resolution full-field-of-view (FFOV) scans with high-resolution scans of specific interior volumes. High-resolution datasets were reconstructed using ZEISS DeepRecon Pro [10, 51], a DL-based 3D reconstruction method that effectively reduces noise and improves image quality. The low-resolution FFOV dataset was then upscaled using DeepScout, a DL-based workflow recently integrated into 3D XRM workflows by ZEISS [52, 53]. While DeepRecon introduces convolutional neural networks trained to generate 3D reconstructed volumes with improved image quality through edge-preserving noise reduction, DeepScout focuses on enhancing the 3D XRM spatial resolution of large-volume datasets without compromising the FOV. By training a deep convolutional neural network on pairs of low- and high-resolution images of the same sample, DeepScout derives a spatially varying effective point spread function, enabling the upscaling of low-resolution scans into high-resolution images.

DeepScout addresses the traditional resolution-volume trade-off, enabling detailed defect detection and microstructural analysis in various materials, such as those used in AM. It also mitigates imaging challenges such as system instability and detector blurring by incorporating spatial priors and high-order voxel-based image registration. This results in improved resolution, noise reduction, and minimized artifacts, facilitating faster acquisition of high-resolution datasets in 3D XRM [54, 55]. By reducing background noise and enhancing image contrast, as illustrated in Fig. 14, DeepScout significantly improves the clarity and detail of the reconstructed images while preserving finer morphological details of voids and unsintered powder. Additionally, higher-resolution XRM scans processed with DeepRecon algorithms enable the clear visualization of cracks, small voids, and satellite particles.

Reconstructions from low-resolution (LR) scans, collected at 8 µm/voxel (Fig. 14), served as input for the DL-based noise reduction and resolution recovery processes. High-resolution (HR) scans, acquired at 3.5 µm/voxel, revealed small pores that were difficult to detect in LR scans. These HR scans were used to train the resolution recovery DL model, which generated the upscaled dataset at 3.5 µm/

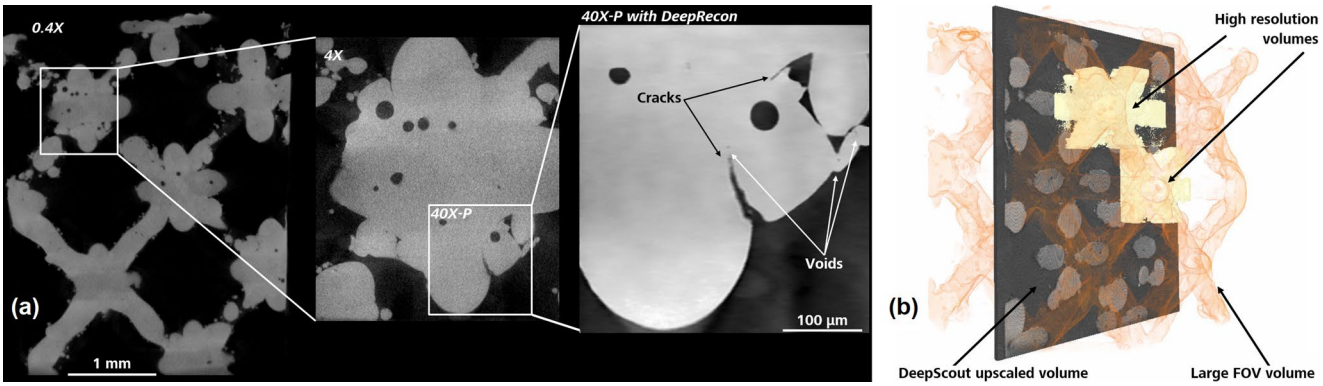

Fig. 13 AM Inconel 718 lattice structure scanned utilizing the RaaD capabilities of a 3D XRM (ZEISS Xradia 630 Versa). (**a**) Cross-sectional views captured with increasing magnification, starting from a 0.4X objective lens, progressing to 4X, and culminating in a 40X zoom-in. A reconstruction using a DL-based algorithm is presented for the 40X image. (**b**) Higher resolution information is upscaled across the entire 3D volume using DL-based reconstruction

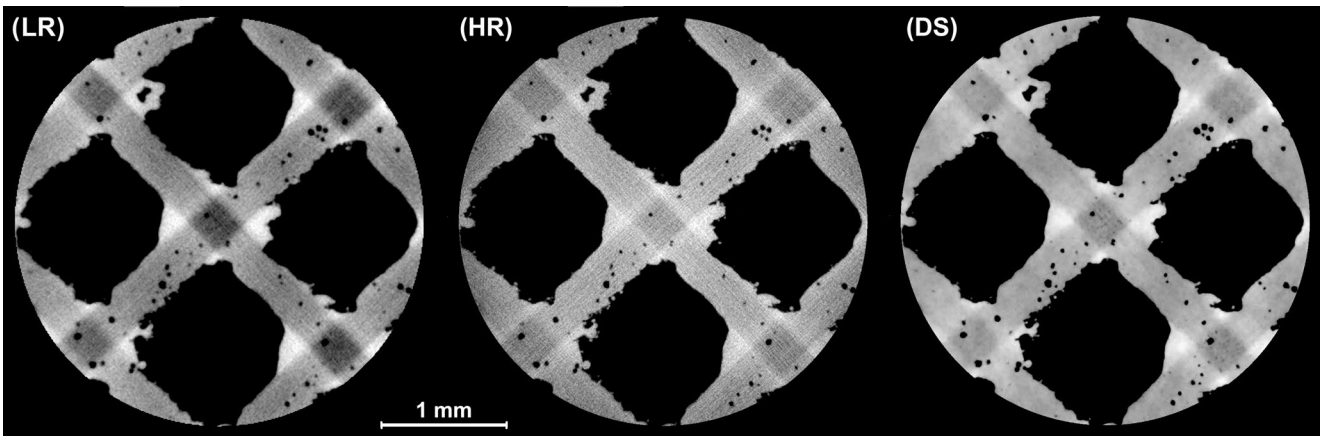

Fig. 14 Comparison of XRM reconstructed cross-sections from the interior volume of an Inconel 718 lattice sample, also depicted in Figure 13. Low-resolution (LR) data were collected at a resolution of 8 µm/voxel and reconstructed using an FDK algorithm. High-resolution (HR) slice data were collected at 3.5 µm/voxel and reconstructed with FDK. Resolution recovery was applied to the LR data using DeepScout (DS), which was trained on HR data. The LR and DS images were circularly cropped to emphasize the region of interest from the HR image

voxel resolution, referred to as the 'DeepScout'(DS) dataset, as shown in Fig. 14. The results show significant improvements in image quality and resolution when transitioning from LR to DS. The DeepScout algorithm enhances edge detection and delivers substantial improvements in spatial resolution, feature recovery, and denoising. Quantitatively, up to 60% more pores were detected in DS compared to LR, with most pores falling within the 15–30 µm diameter range. The HR image confirms that the actual number of pores is indeed higher than what the LR image reveals, indicating that DS effectively refines porosity statistics.

DeepScout also enhances the morphological details of larger pores, attributed to the use of smaller voxels. Although beam hardening artifacts, such as dark streaks and bright edges, cannot be fully corrected (see Fig. 14, particularly in regions where multiple lattice nodes align along certain X-ray transmission paths), DeepScout recovers void details effectively. By incorporating DeepRecon into its processing pipeline, DeepScout inherently reduces noise. In high-noise regions, such as lattice nodes, detecting small pores is particularly challenging due to interference from neighboring noisy pixels. However, the combination of noise reduction and resolution recovery enables better definition of these voids. Challenges in segmenting and quantifying air-connected voids can potentially be addressed using advanced techniques like 3D watershed methods combined with mask subtraction.

Once trained, the DS model can upscale larger sample volumes efficiently, as illustrated in Fig. 15(a-c). These 3D-rendered views compare conventional and DL-based reconstructions. Void segmentation and visualization were performed using DragonFly 3D World ZEISS edition software with simple thresholding methods. The DeepScout upscaled reconstruction (Fig. 15(c)) detects nearly three

times more pores than the conventional reconstruction (Fig. 15(a)). This capability highlights the potential of combining 3D XRM hardware with DL-based reconstruction for advanced AM characterization. The ability to upscale large volumes to high resolutions enables detailed parametric studies with improved sample statistics in less time compared to traditional methods. This approach accelerates time-to-results by requiring fewer scans to extract high-resolution data across the entire FOV and enhances instrument efficiency by minimizing redundant data acquisition.

Access to high resolution across the entire FOV allows researchers to probe all parts of a sample equally, eliminating the need for traditional top-down investigative routines. Conventional X-ray microscopy often relies on low-resolution imaging to "volumes of interest" for subsequent high-resolution scanning. This approach can fail at identifying key regions of interest when low-resolution scans lack sufficient contrast or morphological differences, particularly for sub-micron pores that remain undetected. Additionally, the time required for high-resolution analysis scales linearly with the number of probe sites chosen. In contrast, DeepScout approach enables a single-shot approach of the entire volume based on a deep-learning model trained on a single high-resolution dataset.

DeepScout reconstruction results were validated by imaging a coincident cross-section of the sample using femtosecond laser ablation and SEM imaging (ZEISS Crossbeam 550 Laser). As shown in Fig. 16, the void distribution observed in the SEM image of the physically cross-sectioned sample closely matches the distribution detected in the DeepScout data. Notably, finer details, such as distinguishing filled versus unfilled voids and detection of smaller voids, were evident in the DeepScout data but indiscernible in conventional 3D XRM scans. These findings demonstrate that DL reconstruction methods effectively recover resolution lost in low-resolution scans while introducing minimal artifacts. To the authors' knowledge, no other non-destructive methods are capable of imaging such small interior pores.

For further validation, destructive techniques such as mechanical serial sectioning or focused ion beam SEM (FIB-SEM) milling could be considered. However, these methods have limitations, including resolution constraints, labor-intensive preparation, and potential alteration of voids during processing. For the data presented in Fig. 16, a correlative microscopy approach was employed to target features identified in non-destructive 3D scans. The 3D data provided critical navigational guidance, with surface features in the rendering acting as reference points (fiducials) to guide precise sectioning. This workflow combines rapid laser ablation with accurate FIB sectioning, ensuring high precision and reliability. This method has been rigorously validated across diverse sample types and is widely recognized as a reliable workflow for users of ZEISS instruments. While the process can be adapted for use with other microscope brands, it may be less efficient and reliable due to the lack of a fully integrated system for seamless data flow and precise navigation. The integration of 3D data with sectioning tools is essential for achieving the level of accuracy demonstrated in this approach.

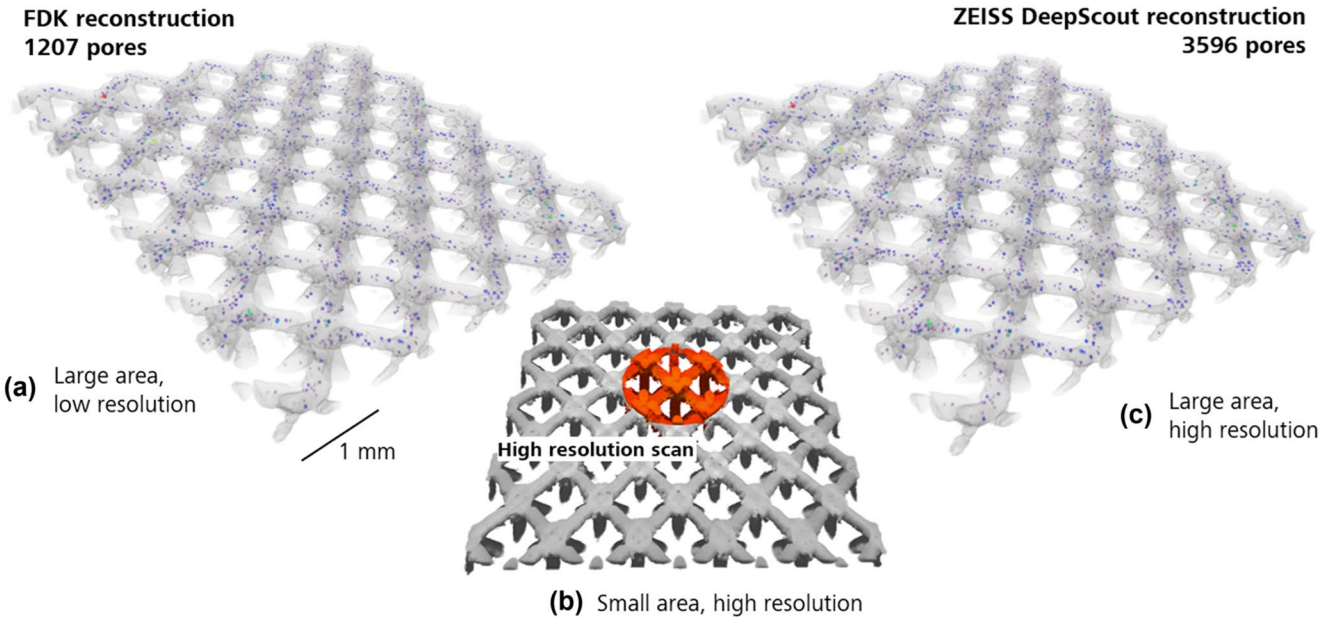

Fig. 15 (**a**) 3D rendering of the Inconel lattice structure scanned at low resolution in grey. (**b**) The orange sub-volume highlights the high-resolution region of interest. (**c**) A large section of the lattice structure, with resolution recovery applied, rendered to illustrate the enhancement in captured internal porosity following DeepScout reconstruction

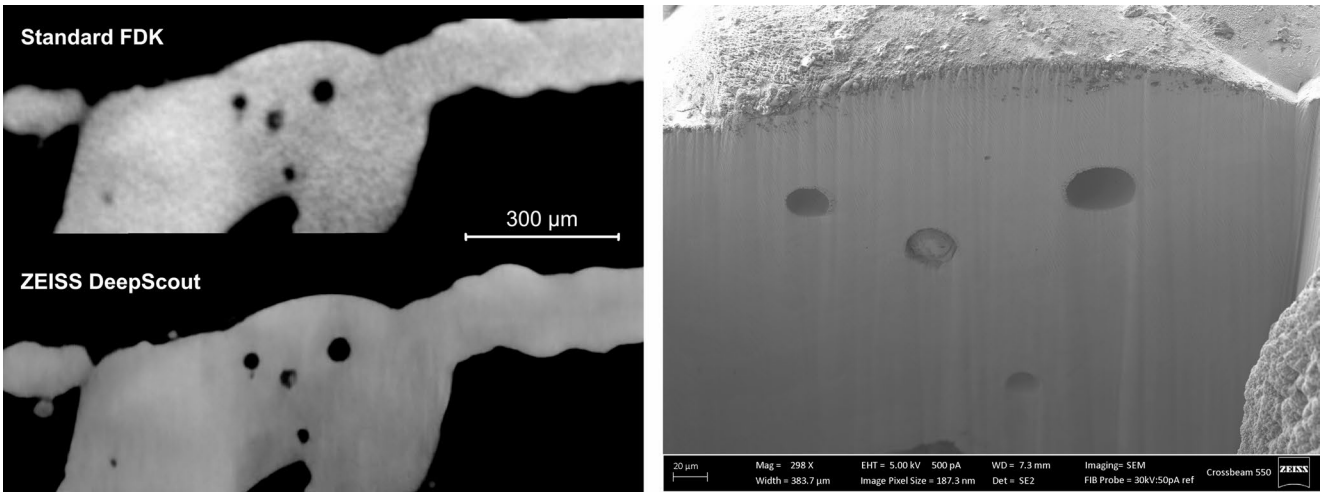

Fig. 16 Comparison of two XRM cross-sectional slices (left) reconstructed using standard FDK vs the advanced DeepScout algorithm. Validation of the 2D XRM reconstructed images is done by juxtaposing them with an SEM image (right) of the Laser FIB-sectioned region, captured at the same location as the XRM reconstructed slices. Notably, the four prominent voids, including a central void filled with unmelted powder, are distinctly observable in both the DeepScout and SEM datasets

The results presented in this study demonstrate that incorporating DL-based reconstruction algorithms, such as DeepRecon and DeepScout, enables noise-free and resolution-recovered data, offering new opportunities for efficient and reliable AM characterization. This is a critical step toward advancing the understanding of the relationship between processing parameters, microstructure, and mechanical properties. Further evaluation of DeepScout performance, focusing on resolution differences and recoverable feature sizes, is presented elsewhere [56]. Overall, DeepScout has demonstrated significant improvements in resolution recovery and feature enhancement, making a robust and versatile tool for materials characterization, particularly in AM. The results indicate that DeepScout consistently outperforms other methods in terms of feature recovery, accuracy, and reduced artifacts, effectively bridging the gap between low and high-resolution imaging and enabling detailed analysis of complex materials. While DeepScout excels in enhancing spatial resolution, its performance depends on the quality and diversity of the training data, which is essential for optimal generalizability and accuracy in feature recovery. As an example, any misregistration between the low resolution and high-resolution training images can impact performance. It is designed to handle resolution ratios up to 7:1, and while it performs well within this range, exploring higher ratios may present challenges, including the potential for hallucinations—spurious features that do not exist in the original images. The algorithm does require increased computational effort for training (3–4 h) and inference (0.5 to 2 h) on a professional NVIDIA graphics workstation, as well as upsampled results require increased disk space storage depending on the upsampling ratio. While the operations of the neural network behind the DeepScout may not always be easily interpretable, ongoing research aims to enhance its usability and generalizability across various materials and imaging conditions.

6 Conclusions

This paper explores advancements in multiscale characterization of additive manufacturing (AM) components using X-ray computed tomography (XCT), 3D X-ray microscopy (XRM), and deep learning (DL) techniques. These methods address key challenges in inspecting complex internal geometries and detecting defects critical to ensuring structural integrity and performance. Modern XCT and 3D XRM systems, particularly those equipped with RaaD capabilities, significantly enhance spatial resolution and imaging quality, enabling detailed visualization of internal structures and defects that traditional methods often fail to detect. Applications include internal defect detection, surface roughness evaluation, and process parameter optimization.

DL-based reconstruction methods, such as Simurgh, DeepRecon, and DeepScout, have significantly enhanced XCT workflows by reducing scan times while preserving high-frequency information, thereby improving resolution and defect detection capabilities. These advancements improve image quality, enable accurate porosity characterization, and overcome traditional limitations in resolution and FOV. By integrating XCT, XRM, and DL techniques, researchers can identify and analyze porosity and defects across multiple scales, generating dense statistical data for accurate analysis from sub-micrometer to macroscopic levels. This multiscale imaging approach provides critical insights into

the relationships between defects, material properties, and mechanical performance.

DL-enhanced workflows also streamline the rapid assessment and optimization of AM parameters, enabling efficient analysis of numerous samples. This supports quality control and accelerates the development of new alloys and components. Machine learning-driven optimization of XCT and XRM techniques improves reliability and efficiency in characterizing AM components, deepening understanding of the links between processing parameters, microstructure, and mechanical properties. High-throughput workflows enabled by XCT and DL have reduced analysis times from weeks to days, allowing for faster refinement of parameters such as laser power, velocity, and hatch spacing to improve part quality and process repeatability. Additionally, high-resolution XRM scans facilitate non-destructive assessment of internal surfaces and trapped powder particles, offering valuable insights into defect formation mechanisms and their impact on structural integrity.

Despite challenges in generalizing DL models to diverse materials and imaging conditions, the demonstrated success of these methods underscores their transformative potential. As these technologies evolve, they will play an increasingly vital role in advancing AM, enabling the production of reliable, high-performance components for demanding industrial applications.

This paper also highlights the importance of multiscale imaging approaches that integrate data from XCT, XRM, and SEM to provide a comprehensive view of AM components and correlate microstructural features with performance. Future research should focus on automating DL training, enhancing model robustness, and exploring uncertainty quantification and explainable artificial intelligence to improve DL-based non-destructive testing. Expanding the generalizability of DL models across various materials and imaging conditions is essential for broader adoption in AM.

In conclusion, the integration of advanced XCT, 3D XRM, and DL techniques represents a significant leap forward in the characterization and quality control of AM parts. These methods provide valuable insights into microstructural features and their performance correlations across multiple length scales, driving innovations that enhance material properties, optimize production processes, and deliver higher-quality AM products.

Acknowledgements This work was co-authored by UT-Battelle, LLC under contract DE-AC05-00OR22725 with the US Department of Energy (DOE) and supported by the DOE Office of Energy Efficiency and Renewable Energy (EERE), Advanced Materials & Manufacturing Technologies Office (AMMTO). The US government retains and the publisher, by accepting the article for publication, acknowledges that the US government retains a nonexclusive, paid-up, irrevocable, worldwide license to publish or reproduce the published form of this manuscript, or allow others to do so, for US government purposes. DOE will provide public access to these results of federally sponsored research in accordance with the DOE Public Access Plan (http://energy.gov/downloads/doe-public-access-plan).

Author Contributions H.V-G. authored the primary manuscript text, while all authors contributed design of experiments, analysis, and the preparation of the figures and participated in the manuscript review and editing process.

Funding A.Z., O.R., and Z.S. received support from the US Department of Energy (DOE), Advanced Materials & Manufacturing Technologies Office (AMMTO), as well as DOE Technology Commercialization Fund (TCF-21-24881). Funding for the work related to DeepRecon and DeepScout was provided by Carl Zeiss X-ray Microscopy. The funders played no part in the study's design, data collection and analysis, decision to publish, or manuscript preparation. The open access publication fee for this article has been paid by Carl Zeiss Industrielle Messtechnik GmbH.

Data Availability The data supporting the findings of this study are available from the authors upon reasonable request.

Declarations

Conflicts of interest The authors H.V-G., P.B., A.A., Y.T., N.J., H.B. J.S., and E.D.S. are employees of ZEISS.

References

1. Thompson, A., Maskery, I., Leach, R.K.: X-ray computed tomography for additive manufacturing: A review. Meas. Sci. Technol. **27**(17pp), 072001 (2016)
2. Hassen, A.A., Kirka, M.M.: Additive manufacturing: The rise of a technology and the need for quality control and inspection techniques. Mater. Eval. **76**(4), 439–453 (2018)
3. du Plessis, A., Yadroitsev, I., Yadroitsava, I., Le Roux, S.G.: X-Ray microcomputed tomography in additive manufacturing: A review of the current technology and applications. 3D Print. Additive Manuf. 5(3), 227–247 (2018). https://doi.org/10.1089/3dp.2018.0060
4. Villarraga-Gómez, H., Lee, C., Corbett, T., Tarbutton, J.A., Smith, S.T.: Assesing additive manufacturing processes with X-ray CT metrology, in *ASPE Spring Topical Meeting*, Raleigh, NC, (2015)
5. Villarraga-Gómez, H., Peitsch, C.M., Ramsey, A., Smith, S.T.: The role of computed tomography in additive manufacturing. in In: 2018 ASPE and Euspen Summer Topical Meeting: Advancing

Precision in Additive Manufacturing, pp. 201–209. Lawrence Berkeley National Laboratory, Berkeley, California (USA) (2018)
6. Villarraga-Gómez, H., Frederick, C., Brackman, P., Andreyev, A., Trenikhina, Y., Johnson, N., Bale, H.: Non-destructive characterization of additive manufacturing components with computed tomography and 3D X-ray microscopy, in *13th Conference on Industrial Computed Tomography (iCT)*, Wels, Austria, (2024)
7. Villarraga-Gómez, H., Herazo, E.L., Smith, S.T.: X-ray computed tomography: From medical imaging to dimensional metrology. Precis. Eng. **60**, 44–569 (2019)
8. Villarraga-Gómez, H., Morse, E.P., Smith, S.T.: Assessing the effect of penetration length variations on dimensional measurements with X-ray computed tomography. Precis. Eng. **79**, 146–163 (2023)
9. Villarraga-Gómez, H., Begun, D.L., Bhattad, P., Mo, K., Norouzi Rad, M., White, R.T., Kelly, S.T.: Assessing rechargeable batteries with 3D X-ray microscopy, computed tomography, and nanotomography. Nondestructive Test. Evaluation. **37**(5), 519–535 (2022)
10. Villarraga-Gómez, H., Crosby, K., Terada, M., Rad, M.N.: Assessing electronics with advanced 3D X-ray imaging techniques, nanoscale tomography, and deep learning. J. Fail. Anal. Prev. **24**, 2113–2128 (2024)
11. Villarraga-Gómez, H., Kotwal, N., Parwani, R., Weiß, D., Krenkel, M., Kimmig, W.: Graf vom hagen, improving the dimensional accuracy of 3D X-ray microscopy data. Meas. Sci. Technol. **33**(7), 074002, 10 (2022)
12. Bellens, S., Guerrero, P., Vandewalle, P., Dewulf, W.: Machine learning in industrial X-ray computed tomography– a review. CIRP J. Manufact. Sci. Technol. **51**, 324–341 (2024)
13. Ziabari, A., Venkatakrishnan, S.V., Snow, Z., Lisovich, A., Sprayberry, M., Brackman, P., Frederick, F., Bhattad, B., Graham, S., Bingham, P., Dehoff, R., Plotkowski, A., Paquit, V.: Enabling rapid X-ray CT characterisation for additive manufacturing using CAD models and deep learning-based reconstruction. Npj Comput. Mater. **9**(91), 10 (2023)
14. Ziabari, A., Venkatakrishnan, S., Dubey, A., Lisovich, A., Brackman, B., Frederick, C., Bhattad, P., Bingham, P., Plotkowski, A., Dehoff, R., Paquit, V.: Simurgh: A framework for cad-driven deep learning based x-ray ct reconstruction, in *IEEE International Conference on Image Processing (ICIP)*, Bordeaux, France, pp. 3836-3867, (2022)
15. Laboratory, O.R.N.: Simurgh: AI-assisted CT scan optimization, [Online]. Available: https://www.ornl.gov/technology/90000193. [Accessed May 2025]
16. Ziabari, A., Bedhief, M.H., Rahman, O., Venkatakrishnan, S., Brackman, P., Katuch, P.: Combining deep learning and scatterControl for high-throughput X-ray CT based non-destructive characterization of large-scale casted metallic components, in *14th International Conference on Industrial Computed Tomography (iCT)*, Antwerp, Belgium, (2025)
17. Rahman, O., Venkatakrishnan, S.V., Snow, Z., Brackman, P., Feldhausen, T., Dehoff, R., Paquit, V., Ziabari, A.: Neural Network-based Single-material Beam Hardening Correction for X-ray CT in Additive Manufacturing, in *17th International Meeting on Fully 3D Image Reconstruction in Radiology and Nuclear Medicine*, Stony Brook, NY, USA, (2023)
18. Palenstijn, W.J., Batenburg, K.J., Sijbers, J.: The ASTRA tomography toolbox, in *13th International Conferenceon Computational and Mathematical Methodsin Science and Engineering*, Almería, Spain, (2013)
19. Zhu, J.Y., Park, T., Isola, P., Efros, A.A.: Unpaired Image-to-Image Translation Using Cycle-Consistent Adversarial Networks, in *IEEE International Conference on Computer Vision*, Venice, Italy, (2017)
20. Ziabari, A., Rahman, O., Franklin, R., Sprayberry, M., Peles, A.: High-Throughput Characterization Tools/Algorithms To Outline Porosity Variability In AM Samples As A Function OF Processing Conditions, ORNL/SPR-2025/3776, Oak Ridge National Laboratory, Oak Ridge, TN, USA, (2025)
21. Snow, Z., Scime, L., Ziabari, A., Fisher, B., Paquit, V.: Scalable in situ non-destructive evaluation of additively manufactured components using process monitoring, sensor fusion, and machine learning. Additive Manuf. **78**, 103817 (2023)
22. Ziabari, A., Snow, Z., Ortega, J., Paquit, V.: Deep Learning Based Sparse X-ray CT Image Reconstruction of Thick and Complex AM Parts Made of High-Density Nickle Super-Alloys, in *International Workshop On Electromagnetic Nondestructive Evaluation (ENDE)*, Knoxville, TN, USA, (2025)
23. Feldkamp, L.A., Davis, L.C., Kress, J.W.: Practical cone-beam algorithm. J. Opt. Soc. Am. A. **1**(6), 612–619 (1984)
24. Villarraga-Gómez, H., Smith, S.T.: Effect of the number of projections on dimensional measurements with X-ray computed tomography. Precis. Eng. **66**, 445–456 (2020)
25. Jerri, A.J.: The Shannon Sampling Theorem—Its Various Extensions and Applications: A Tutorial Review, in *Proc. of the IEEE, Vol: 65, no 11*, (1977)
26. Fieser, D., Lawton, M., Bahl, S., Ziabari, A., Plotkowski, A., McDonald, E., Babu, S., Hu, A.: Processing, mechanical properties, and microstructure characterization of Crack-free AlCe-Ni alloys with laser additive manufacturing. Under Rev., (2025)
27. Da, G., Lambert-Garcia, R., ocine, S., Fan, X., Greenhalgh, H., Shahani, R., Majkut, M., Rack, A., Lee, P.D., Alex, C.L., Leung: Correlative spatter and vapour depression dynamics during laser powder bed fusion of an Al-Fe-Zr alloy. Int. J. Extreme Manuf. **6**(5), 055601 (2024)
29. Team, O.D.: ICP registration, in Open3D: A Modern Library for 3D Data Processing, [Online]. Available: https://www.open3d.org/docs/latest/tutorial/pipelines/icp_registration.html. [Accessed May 2025]
30. Bhattad, P., Sarraf, A.: Addressing variable print quality in am using novel deep-learning based CT solutions, in *RAPID+TCT conference*, Chicago, IL, USA, (2023)
31. Ziabari, A.K., Rahman, O., Pisa, G., Shahani, R., Stoppiglia, H., Panourgias, G., Brackman, P., Santos, E., Frederick, C., Requena, G., Bugelnig, K., Boller, E.: A comparative study of non-destructive evaluation techniques: ultrasonic testing, X-ray computed tomography, and large-field-of-view synchrotron tomography, in *ASTM ICAM conference*, Atlanta, (2024)
32. Robsertson, J., Poly, S., Shahani, R.: Validating porosity prediction for aluminum laser powder bed fusion components, in *RAPID+TCT conference*, Detroit, MI, USA, (2025)
33. Pramanik, A., Venkatakrishnan, S.V., Rahman, O., Ziabari, A.: A learnt half-quadratic splitting-based algorithm for fast and high-quality industrial cone-beam CT reconstruction, *arXiv e-prints*, p. arXiv:2501.13128, (2025)
34. Pramanik, A., Rahman, O., Venkatakrishnan, S.V., Ziabari, A.: A fast, scalable, and robust deep learning-based iterative reconstruction framework for accelerated industrial cone-beam X-ray computed tomography. ArXiv e-prints. (2025). arXiv:2501.13961
35. Slotwinski, J.A., Garboczi, E.J., Stutzman, P.E., Ferraris, C.F., Watson, S.S., Peltz, M.A.: Characterization of metal powders used for additive manufacturing. J. Res. Natl. Inst. Stand. Technol. **119**, 460–493 (2014)
36. Kim, F.H., Moylan, S.P., Garboczi, E.J., Slotwinski, J.A.: Investigation of pore structure in Cobalt Chrome additively manufactured parts using X-ray computed tomography and three-dimensional image analysis. Additive Manuf. **17**, 23–38 (2017)
37. DebRoy, T., Wei, H.L., Zuback, J.S., Mukherjee, T., Elmer, J.W., Milewski, J.O., Beese, A.M., Wilson-Heid, A., De, A., Zhang, W.:

Additive manufacturing of metallic components– Process, structure and properties. Prog. Mater. Sci. **92**, 112–224 (2017)
38. Sames, W.J., List, F.A., Pannala, S., Dehoff, R.R., Babu, S.S.: The metallurgy and processing science of metal additive manufacturing. Int. Mater. Rev. **65**(5), 315–360 (2016)
39. Sutton, A.T., Kriewal, C.S., Leu, M.C., Newkirk, J.W.: Powders for additive manufacturing processes: Characterization techniques and effects on part properties, in *Proc.of 26th Annual International Solid Freeform Fabrication Symposium–An Additive Manufacturing Conference*, Austin, Texas (USA), pp. 1004-1030, (2016)
40. Villarraga-Gómez, H., Ramsey, A., Seifi, M., Peitsch, C.M.: The role of X-ray computed tomography in additive manufacturing. in In: 2018 ASPE and Euspen Summer Topical Meeting: Advancing Precision in Additive Manufacturing. Lawrence Berkeley National Laboratory, Berkeley, California (USA) (2018)
41. Slotwinski, J.A., Garboczi, E.J., Hebenstreit, K.M.: Porosity measurements and analysis for metal additive manufacturing process control. J. Res. Natl. Inst. Stand. Technol. **119**, 494–528 (2014)
42. Wits, W.W., Carmignato, S., Zanini, F., Vaneker, T.H.: Porosity testing methods for the quality assessment of selective laser melted parts. CIRP Ann. **65**(1), 201–204 (2016)
43. Hermanek, P., Zanini, F., Carmignato, S., Savio, E.: X-ray computed tomography for additive manufacturing: Accuracy and porosity measurements, in *ASPE/euspen 2016 Summer Topical Meeting*, Raleigh, NC (USA), (2016)
44. Seifi, M., Gorelik, M., Waller, J., Hrabe, N., Shamsaei, N., Daniewicz, S., Lewandowski, J.: Progress towards metal additive manufacturing standardization to support qualification and certification. J. Minerals Met. Mater. Soc. **69**(3), 439–455 (2017)
45. Adair, D., Kirka, M.,Ryan, D.: Additive Manufacture of Prototype Turbine Blades for Hot-Fired Engine Performance Validation Trials, in *Proc. of the ASME Turbo Expo*: Turbomachinery Technical Conference and Exposition, Phoenix, AZ, USA, paper no GT2019-90966, V006T24A012, pp. 1-8, 2019. (2019)
46. Gallardo, D., Lucía-Candela, D., Jiménez, R., Torralba, M., Albajez, J.A., Yagüe-Fabra, J.A.: X-Ray computed tomography performance in metrological evaluation and characterisation of polymeric additive manufactured surfaces. Additive Manuf. **75**, 103754 (2023)
47. Lifton, J.J., Liu, Y., Tan, Z.J., Mutiargo, B., Goh, X.Q., Malcolm, A.A.: Internal surface roughness measurement of metal additively manufactured samples via x-ray CT: The influence of surrounding material thickness. Surf. Topogr. Metrol. Prop. **9**, 035008 (2021)
48. Klingaa, C.G., Dahmen, T., Baier, S., Mohanty, S., Hattel, J.H.: X-ray CT and image analysis methodology for local roughness characterization in cooling channels made by metal additive manufacturing. Additive Manuf. **32**, 101032 (2020)
49. Lettenbauer, H., Lotze, A., Kunzmann, S.: Method and device for identifying material boundaries of a test object. United States Patent US. **8**(045,806 B2), 25 (Oct. 2011)
50. Reinhart, C.: Industrial computer tomography– A universal inspection tool, in *17th World Conference on Nondestructive Testing*, Shanghai, China, (2008)
51. Andrew, M., Omlor, L., Andreyev, A., Sanapala, R., Khoshkhoo, M.S.: New technologies for X-ray Microscopy: phase correction and fully automated deep learning based tomographic reconstruction, in *Proc. SPIE 11840, Developments in X-Ray Tomography XIII, 118400I*, San Diego, CA, USA, (2021)
52. Andrew, M., Andreyev, A., Yang, F., Terada, M., Gu, A., White, R.: Fully automated deep learning-based resolution recovery, in *Proc. SPIE 12242, Developments in X-Ray Tomography XIV, 122420M*, San Diego, CA, USA, (2022)
53. Johnson, N.S., Trenikhina, Y., Bale, H., Kelly, S.: Deep-learning models enable high-resolution reconstruction of large-volume x-ray microscopy datasets, in *Proc. SPIE 13152, Developments in X-Ray Tomography XV, 131520U*, San Diego, CA, USA, (2024)
54. Villarraga-Gómez, H., Andreyev, A., Andrew, M., Bale, H., Sanapala, R., Terada, M., Gu, A., Johnson, B., Omlor, L.: and C. Graf vom Hagen, Improving scan time and image quality in 3D X-ray microscopy by deep learning reconstruction techniques, in *Proc. of 35th ASPE Annual Meeting, Vol 75, pp. 361-366*, Minneapolis, MN, USA, (2021)
55. Villarraga-Gómez, H., Norouzi Rad, M., Andrew, M., Andreyev, A., Sanapala, R., Omlor, L.: and C. Graf von Hagen, Improving throughput and image quality of high-resolution 3D X-ray microscopes using deep learning reconstruction techniques, in *Proc. of 11th Conference on Industrial Computed Tomography*, Wels, Austria, pp. 1-6, (2022)
56. Bukka, V.V.R., Xu, M., Andrew, M., Andreyev, A.: Assessment of deep-learning-based resolution recovery algorithm relative to imaging system resolution and feature size. Methods Microscopy, pp. 1–9, (2025)